Chapter 14
Probing the Potential of Neutron Imaging for Biomedical and Biological Applications

K.L. Watkin, H.Z. Bilheux, and J.F. Ankner

Abstract Neutron imaging of biological specimens began soon after the discovery of the neutron by Chadwick in 1932. The first samples included tumors in tissues, internal organs in rats, and bones. These studies mainly employed thermal neutrons and were often compared with X-ray images of the same or equivalent samples. Although neutron scattering is widely used in biological studies, neutron imaging has yet to be exploited to its full capability in this area. This chapter summarizes past and current research efforts to apply neutron radiography to the study of biological specimens, in the expectation that clinical and medical research, as well as forensic science, may benefit from it.

Keywords Biology · Neutron imaging · X-ray imaging · Biomedical · Contrast agent · Thermal neutrons · Epithermal neutrons · Small gadolinium particulate oxide (SPGO)

14.1 Introduction

Although carbon dominates the chemistry of biological tissues, hydrogen atoms are the most abundant. Protons (^{1}H) scatter thermal neutrons more strongly than any other nuclei. These two facts ensure that hydrogen is the primary contributor to neutron contrast in biological materials. In addition, since neutrons interact with the nucleus, deuterium (^{2}H) exhibits quite different scattering properties from ^{1}H. These contrast differences are already exploited in neutron scattering and imaging and can readily be applied in a biomedical context.

The principle of neutron imaging is based on the attenuation, via both scattering and absorption, of a directional neutron beam by the matter through which it passes. Neutron imaging is complementary to, rather than competitive with, X-ray techniques. X-rays are scattered and absorbed by electrons, so absorption and

K.L. Watkin (✉)
University of Illinois, College of Applied Health Science, 901 So. Sixth, Champaign, IL 61821, USA
e-mail: watkin@uiuc.edu

I.S. Anderson et al. (eds.), *Neutron Imaging and Applications*, Neutron Scattering Applications and Techniques, DOI 10.1007/978-0-387-78693-3_14,

scattering increase monotonically with atomic number. Neutrons, on the other hand, interact with nuclei and their scattering power does not scale in any regular way with atomic number, as explained in Chapter 1, in this volume.

Neutron radiography and tomography have flourished for engineering and materials science applications, as illustrated in Chapters 11 and 12. Recent studies have been carried out in more biological contexts, such as water transport in plants, as referenced in Chapter 17, and resin uptake in wood [1].

Current probes for medical imaging such as X-rays, ultrasound, magnetic resonance imaging (MRI), and positron emission tomography (PET) principally determine differences in structural anatomy. Ultrasound and functional magnetic resonance imaging (fMRI) also enable the study of functional activity such as changing blood flow, whereas PET highlights specific metabolic functions by measuring the concentration and distribution of a radiopharmaceutical tracer similar to glucose. Neutron imaging is essentially similar in spatial resolution to these techniques, but it exhibits different elemental and isotopic contrasts, which may be advantageous in many cases.

14.2 First Experimental Measurements on Biological Tissues

Initial neutron imaging experiments were conducted in Germany in the mid-1930s [2], soon after the discovery of the neutron by Chadwick in 1932. Thermal neutron imaging of biological tissues was first conducted in the mid 1950s, and work continued through the 1960s. Due to a lack of efficient detectors for epithermal and fast neutrons, experiments during this period were limited to thermal neutron imaging and so used thin biological samples. These were often imaged by passing a beam of thermal neutrons through the sample and exposing a dysprosium- or indium-loaded plate that created beta-emitting radioactive isotopes following neutron capture. The activated plate was then developed using conventional autoradiographic techniques, by placing the plate in close contact with an X-ray-sensitive photographic film.

As a proof-of-principle, plant tissues were successfully imaged with thermal neutrons [3], as illustrated in Fig. 14.1. This work demonstrated the ability of neutrons to detect ^{1}H nuclei in biological tissues. Neutron radiographs of a boral (boron–aluminum alloy) sheet were also produced and compared with their X-ray counterparts to illustrate the complementarity of the two techniques.

Several-millimeter-thick biological samples were imaged with thermal neutrons, as referenced in [4–6]. However, when a much thicker sample such as a human chest was studied, the image (Fig. 14.2) was seriously distorted by both multiple scattering, arising mainly from ^{1}H nuclei, and poor detector spatial resolution. Furthermore, the resolution of the image was mediocre compared with that of an equivalent X-ray radiograph [7].

Although the strong attenuation of thermal neutrons drastically limited both the choice of biological tissues and specimen thickness, various animal tissues were exposed to thermal and cold neutrons and compared with X-ray

Fig. 14.1 Neutron radiography of plant tissues demonstrates the sensitivity of neutrons to hydrogenous materials [3]

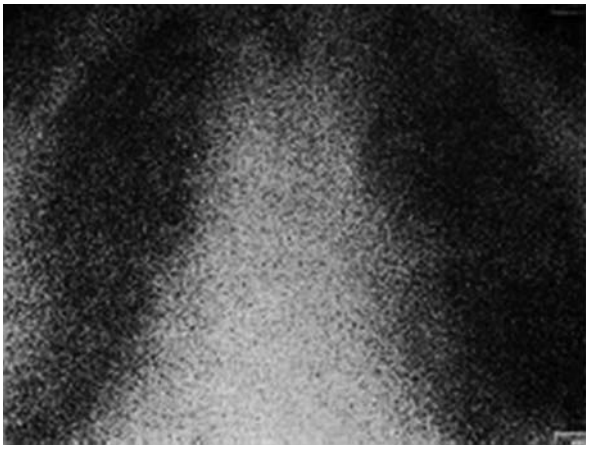

Fig. 14.2 An early thermal neutron radiograph of a human chest was limited by multiple scattering and poor detector spatial resolution [7]

radiographs [6]. Thermal neutron dose was estimated to be equivalent to X-ray dose, whereas incident epithermal dose was predicted to be lower for the same neutron exposure time – epithermal neutrons generally have lower elastic scattering cross sections than thermal neutrons. Gadolinium and indium were commonly used as contrast agents for thermal and epithermal neutron imaging, respectively. A brief discussion of radiation damage due to neutrons can be found in a later section of this chapter.

Figure 14.3 shows images of thin tumor specimens: (A) adenocarcinoma, (B) liposarcoma, and (C) leiomyoma [6]. Thermal neutron images are displayed in the upper row. The control images for each tumor, 20-kV roentgenograms (X-ray images), are shown in the lower row. The greater contrast seen in the neutron images probably arises from differences in hydrogen density, since many tumors appear to have greater hydrogen content than healthy tissues [6].

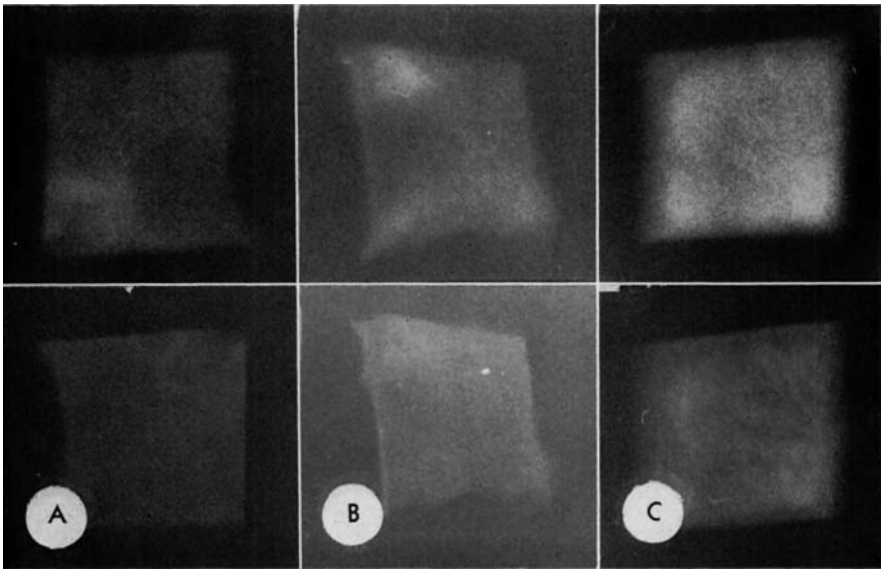

Fig. 14.3 Comparison of tumors imaged with thermal neutrons (*top*) and 20-kV X-rays (*bottom*). The contrast in the neutron radiographs is more pronounced because of higher hydrogen concentrations in tumorous tissue [6]

The complementarity between neutrons and X-rays is better illustrated by images of a rat paw and tail, shown in Fig. 14.4. Although bones are clearly visible in the X-ray radiograph, blood vessels are more prominent in the neutron image. The nasopharynx, which is obscured by bone in the X-ray radiograph, is clearly visible in the epithermal neutron image, as illustrated in Fig. 14.5. Depending on the biological sample and the region(s) of interest, there are significant differences in visible features between X-ray and neutron radiography.

Much of the early interest in neutron imaging of biological tissues was generated by the need to determine the distribution of boron delivery agents being developed for treatment of cancers using boron neutron capture therapy (BNCT). In this method, boron atoms are loaded into cancerous cells, which are then irradiated by neutrons; boron absorbs a neutron and produces an energetic alpha particle and ^{7}Li nucleus, which kill the cell. The thermal neutrons used were either strongly absorbed by the body before reaching the cancerous cells, resulting in high radiological dose, or required highly invasive surgery to expose the cancer more directly to the neutron beam [8]. In the

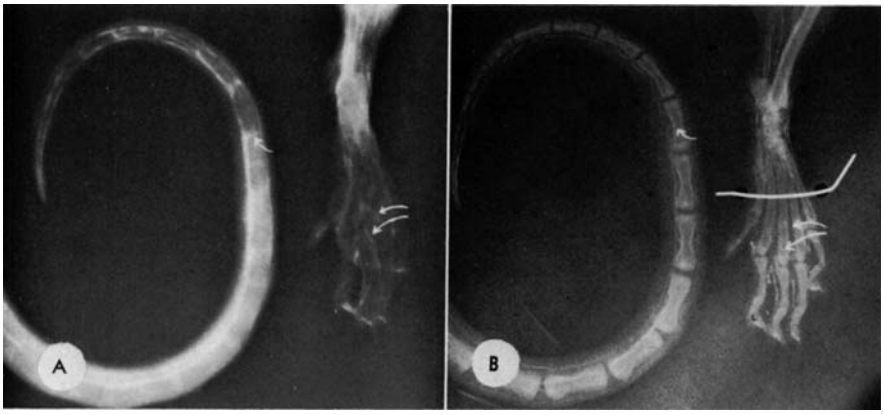

Fig. 14.4 Radiographs of a rat paw and tail using (**A**) thermal neutrons and (**B**) 42-kV X-rays. Gd_2O_3 in oil was used as the contrast agent [6]

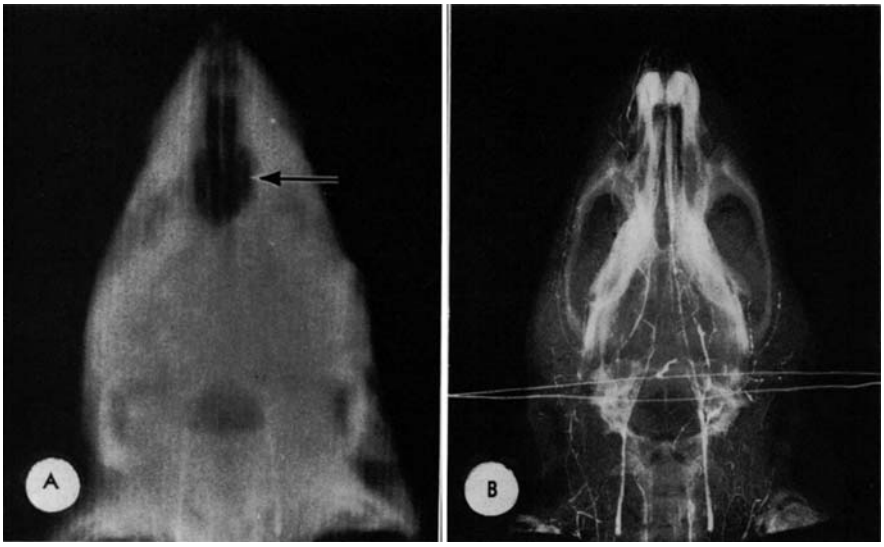

Fig. 14.5 Radiographs of a rat head using (**A**) epithermal (i.e., 0.5 to 2 eV) neutrons and (**B**) 42-kV X-rays. The rat nasopharynx is visible in (A), as indicated by the arrow. Although In_2O_3 was used as a contrast agent, the epithermal neutron flux was not sufficient to demonstrate its contrast capabilities [6]

1990s it was realized that epithermal beams should be more favorable for BNCT, since body tissues act as a natural neutron moderator. Interest in clinical applications reawakened, as did interest in thermal and epithermal imaging of biological tissues.

14.3 Neutron Dosimetry: A Short Overview

As with any imaging method, there is a need to understand and evaluate the benefits and risks of exposing a living subject to neutrons. In order to estimate the potential radiological hazard that neutron imaging poses to soft biological tissues, Monte Carlo simulations of neutron exposure of a simulated human arm were conducted [9]. The conclusions were quite pessimistic. The simulations predicted no effective contrast at given neutron energies of 1 keV, 120 keV, fission spectrum, and 14 MeV. However, the study provided useful information on dose deposition between tissue, bone cortex, and marrow. For example, the calculated neutron dose at 120 keV energy to bone was twice the dose to contiguous soft tissue.

While epithermal (1 eV–0.1 MeV) and fast (>0.1 MeV) neutrons are required to penetrate thick tissues, they do not pose a direct radiological hazard. Rather, hydrogenous tissue moderates these neutrons down to the thermal energy range (<1 eV) at which they can be captured and thereby cause biological damage. Fast neutrons also knock off protons from hydrogenous tissues, creating an additional radiological hazard.

Recently, Monte Carlo simulations for neutron stimulated emission computed tomography (NSECT), an in vivo tomographic spectroscopy using fast neutrons (Chapter 15), demonstrated that the radiation dose deposited in a human abdomen or breast using NSECT would be comparable to the dose from an abdominal CT (computed tomography) exam or a mammogram, respectively [10–12].

Clinical, i.e., small-animal, and pharmaceutical research may benefit the most from epithermal neutron imaging. The exposure of the specimen is a lesser concern in those fields, and imaging may aid medical diagnosis without the risk of radiation exposure.

Recent data on the biological effects of low radiation exposures can be found in Ref. [13]. Information on the biological effects of fast neutrons on biological tissues can be found in Refs. [14, 15].

14.4 Recent Trends

Neutron beams generated by high-energy medical linacs have recently been shown to be sufficiently intense to produce images exhibiting soft-tissue contrast [16]. It was reported that direct thermal neutron imaging was not as contrast-sensitive as indirect neutron imaging (Chapter 5) or fast neutron imaging. Later, neutron radiography of rabbit VX-2 liver cancer using thermal and cold neutron radiography permitted clear observation of hepatic vessels and the VX-2 tumor, with cold neutron imaging being especially effective. The image contrast of this modality enhanced tumor identification compared with absorption-contrast X-ray radiography [17].

Very recently (Figs. 14.6 and 14.7), a study of rat femurs demonstrated the relative strengths of X-ray and neutron imaging. Heavy elements (predominantly calcium and phosphorus in bone) determine X-ray contrast, so the X-ray images highlight the hard bone framework, with the hydrogenous matter being essentially invisible. Neutrons, on the other hand, highlight a relatively uniform distribution of hydrogen throughout the interior and exterior regions of the bone and do not resolve the filaments of trabecular hard bone running through the marrow. Interestingly, the neutron images (Fig. 14.7) show an obvious bone reduction in the decalcified samples – after inorganic compounds are dissolved by soaking in a 15% ethylene diamine tetra acetic acid solution, as expected

Fig. 14.6 Images made by 40-keV X-ray radiography of (**a**) calcified bones (i.e., heated at 600°C for 5 h) and (**b**) natural bones. The distinction between the cortical (surface) and the trabecular (inner) bone regions is evident [18]

Fig. 14.7 Neutron radiographs of rat bones from (**a**) decalcified and (**b**) natural bones [18]

from the egression of mineral material from inside the bone. Post-mortem bone desiccation was also evaluated as a possible forensic tool [18].

Several recent neutron imaging experiments on biological samples have been published, e.g., the remains of an ichthyosaur embryo imbedded in a shell [19], arachnids [20], and insects [21]. Examples of radiographs of other biological specimens can be found at http://neutra.web.psi.ch/gallery/biological.html.

Adult male porcine lung tissue (1.5 mm thick, 1 cm by 1 cm sample size) immersed in formalin was successfully imaged using thermal neutrons. These slices were first extracted from frozen samples from the anatomical region illustrated in Fig. 14.8.

Standard histological techniques were used to allow comparison of neutron and optical images (Fig. 14.9). After neutron exposure, the samples were stained using hematoxylin and eosin stain, which is known to provide good resolution of lung tissue components such as muscle and cartilage.

Although the images in Fig. 14.9 look very similar, the distribution of their pixel intensities can supply a true quantitative comparison. Recently developed software [22] enables automatic integration of multiscale volumes from different imaging modalities through a cyber-based portal imaging system. It was found that 92% of the pixel intensities of these two images match, meaning the pixel-by-pixel intensity between the histological and the neutron images is very similar. These initial results for fixed porcine lung tissue provide significantly more detail than any previously reported images taken with a thermal neutron beam [7]. To compare thermal neutron imaging with X-ray imaging, the specimen was also imaged using microCT, as shown in Fig. 14.10. The microCT measurement was conducted before histological staining and subsequent optical imaging. The gross morphology in all the images is very similar. Cartilage

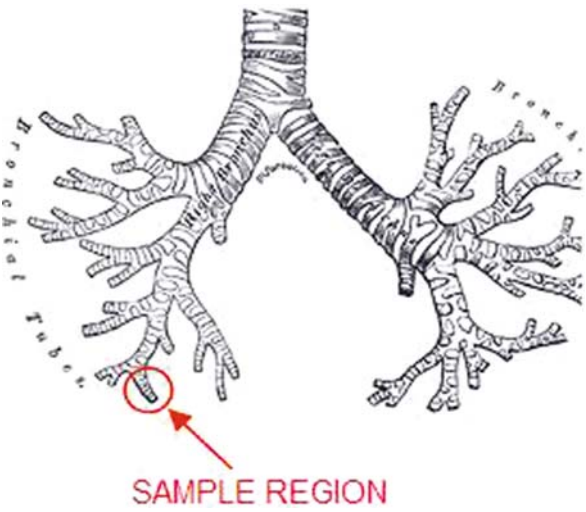

Fig. 14.8 Approximate location of the thin porcine lung specimen imaged using thermal neutrons. Only the lung airways are illustrated

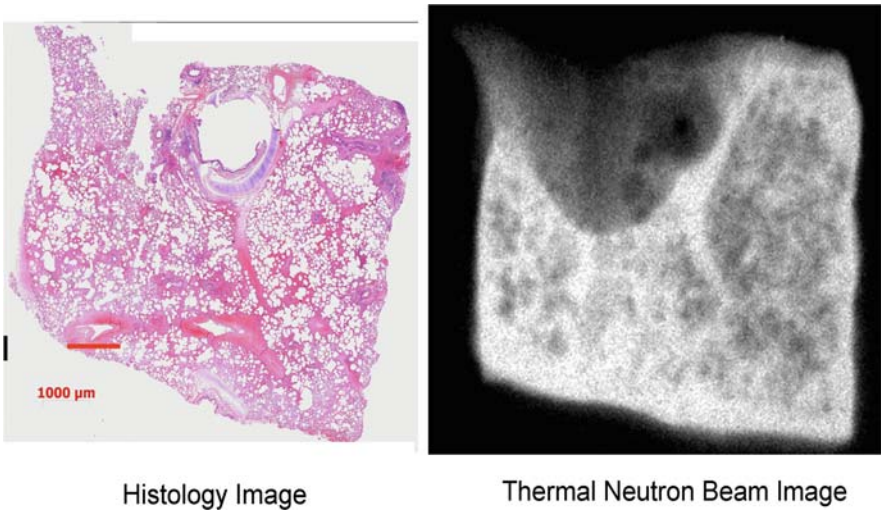

Fig. 14.9 Histological and thermal neutron images of the same section of porcine lung, with a 92% pixel agreement (see text)

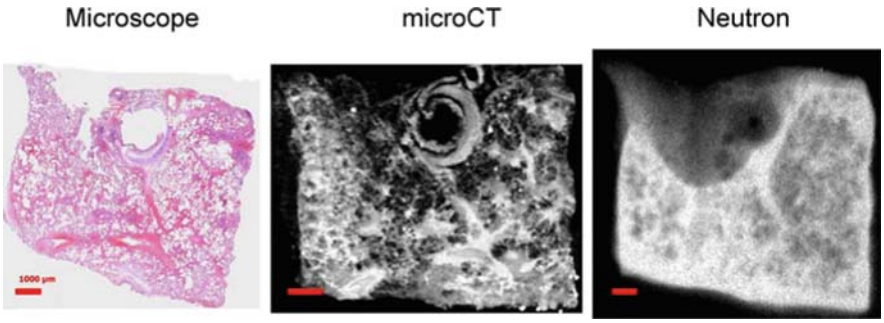

Fig. 14.10 Multimodal images of the same specimen of porcine lung tissue

supporting the airway is clearly visible in each modality, along with differentiation of the alveolar regions, although the greatest definition is seen in the histology images.

In a recent study, the anatomical changes in corn kernels affected by *Aspergillus flavus* fungus were analyzed quantitatively using neutron tomography [23], demonstrating the effectiveness of the technique in identifying the degradation of the biological tissues compared with tissues in uninfected control kernels. Resistant kernels showed no sign of anatomical change. This interesting research shows the sensitivity of neutron radiography to the effects of diseases on biological tissues. The most recent and promising studies are illustrated by tomography of a rat lung [24].

14.5 Small Particulate Gadolinium Oxide (SPGO) Nanoparticles for Targeted and Nontargeted Contrast Enhancement for Future Biomedical Neutron Imaging Applications

There is a great and largely untapped potential for the use of neutrons in biomedical imaging using isotopically labeled marker compounds. Medical compounds incorporating neutron-absorbing isotopes can be targeted to specific organs, such as the heart, to enable neutron imaging of anatomical structure and organ function as well as to deliver radiation doses specifically to tumor sites. Such a system could provide higher-resolution images than PET and more precision in targeting disease. Neutrons may also be used with water-stable SPGO (small particulate gadolinium oxide) nanoparticles [25–27] for targeted or non-targeted contrast enhancement. Neutron imaging through metal – e.g., stents and other metallic objects used for biological purposes – is possible. Small-animal imaging studies, isotopic imaging, and targeted contrast-enhanced imaging are all potential applications.

Recent experiments highlight the biomedical potential of the neutron-sensitive SPGO contrast agent. Dextranized SPGO (10 nm) was injected into the portal vessel of a porcine liver specimen. A thermal neutron radiograph of the thin specimen (~1.5 mm) with the dextranized SPGO highlighting the lumen of the vessel is shown in Fig. 14.11. SPGO particles appear dark because of the high thermal neutron capture cross section of gadolinium.

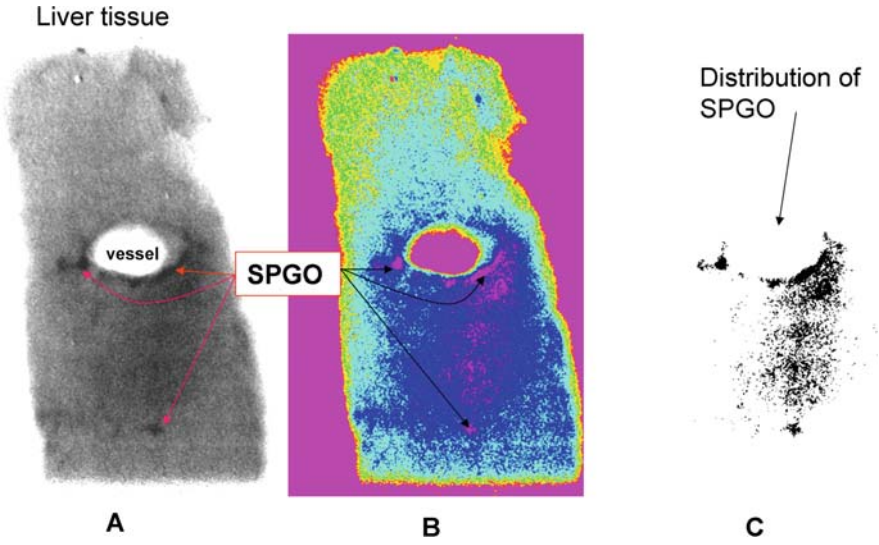

Fig. 14.11 Neutron images of SPGO-doped liver tissue. **A**: original liver specimen; **B**: color-enhanced image of A; **C**: distribution of the SPGO nanoparticles created using simple thresholding techniques

14.6 Summary

Many recent advances in medical imaging are based upon technological advances in computer visualization, refined image projection techniques, and advanced charge-coupled device systems, among others. Although there have been several recent attempts to create small neutron generating systems that may be useful at the laboratory level, the use of larger reactor- and accelerator-based neutron sources with dedicated imaging systems remains the most effective and efficient way to use thermal neutrons for biological tissue imaging.

Neutron radiographs of biological tissues accompanied the first neutron imaging experiments. Neutron imaging of biological samples flourished during the 1960s and 1970s and then largely disappeared until the 1990s. The recent emergence of new techniques and improved detection (e.g., for epithermal neutrons – Chapter 4) are leading to a rejuvenation of the field of neutron imaging.

Neutron imaging of living human subjects still provokes obvious radiological concerns. However, its potential for applications such as clinical research, small-animal imaging, and forensic science needs to be investigated further. The high sensitivity of neutrons to hydrogen atoms should be of benefit for forensic applications, where quantification of water changes in dead tissues is highly important.

Acknowledgments This work is supported by the U.S. Department of Energy. The Oak Ridge National Laboratory Spallation Neutron Source is managed by UT-Battelle, LLC, for the Department of Energy under contract DE-AC05-00OR22725. We would like to thank Dr. John Nemeth of Oak Ridge Associated Universities for financial support of part of this research, under contract DE-AC05-06OR23100. We would also like to thank our many colleagues, especially Daniel Hussey at the National Institute of Standards and Technology Center for Neutron Research and Candice Halbert from Oak Ridge National Laboratory.

References

1. E. Lehmann, S. Hartmann, P. Wyer, *Nucl. Instrum. Meth. A* **542**, 87 (2005).
2. H. Kallman, *Research* **1**, 254 (1947).
3. J. Thewlis et al., *Br. J. Appl. Phys.* 7, 345 (1956).
4. H.L. Atkins, Biological application of neutron radiography, *Mat. Eval.* **23**, 453–458 (1965).
5. Barton, J. P., Some possibilities of neutron radiography, *Phys. Med. Biol.* **9**, 33–42 (1964).
6. M. Brown and P.B. Parks, *Am. J. Roentg.* **106**, 472 (1969).
7. J. Anderson et al., *Br. J. Radiol.* **37**, 957 (1964).
8. R.F. Barth, Coderre, M.G.H.Vicente and T.E.Blue, *Clin. Can. Res.* **11**, 3987–4002 (2005).
9. T.F. Budinger et al., *Phys. Med. Biol.* **16**(3), 439–450 (1971).
10. C.E. Floyd et al., *Phys. Med. Biol.* **51**, 3375–3390 (2006).
11. J.E. Bender, A.J. Kapadia, A.C. Sharma, G.D. Tourassi, B.P. Harrawood, and C.E. Floyd, *Med. Phys.* **34**, 3866–3871 (2007).
12. A.J. Kapadia, A.C. Sharma, J.E. Bender, G.D. Tourassi, C.R. Howell, A.S. Crowell, M.R. Kiser, B.P. Harrawood, R.S. Pedroni, and C.E. Floyd, *IEEE Trans. Nucl. Sci.* **55**(1), 501–509 (2008).

13. F. Zolzer, C. Streffer, *Radiat. Res.* **169**, 207–213 (2008).
14. Health effects of exposure to low levels of ionizing radiation: BEIR V, National Academic Press, ISBN 0-309-03997-5.
15. Introduction to Radiological Physics and Radiation Dosimetry, Wiley-VCH, ISBN 0-471-01146-0.
16. N. Adnani and B.G. Fallone, Neutron imaging using Medical Linacs, *Proceedings of the 22nd Annual EMBS International Conference*, July 23–28, Chicago IL. (2000).
17. Y. Tsuchiya, M. Matsubayashi, T. Takeda, T. Lwin, J. Wu, A. Yoneyama, A. Matsumura, T. Hori and Y. Itai, Imaging of rabbit VX-2 hepatic cancer by cold and thermal neutron radiography *Jpn. J. Appl. Phys.* **42**, 7151–7153 (2003).
18. K.K. Moghaddam, T.T. Taheri, and M. Ayubian, Bone structure investigation using X-ray and neutron radiography techniques, *Appl. Radiat. Isot.* **66**, 39–43 (2008).
19. D. Schwarz, P. Vontobel, E.H. Lehmann, C.A. Meyer, and G. Bongartz, Neutron tomography of internal structures of vertebrate remains: A comparison with X-ray computed tomography, *Palaeontol. Electron.* **8** (2): Art. No. 30A (2005).
20. J.T. Cremer, M.A. Piestrup, H. Park, C.K. Gary, *Appl. Phys. Lett.* **87**, 161913 (2005).
21. B. Allman et al., *Nature* **408**, 158–159 (2000).
22. http://www.ncsa.uiuc.edu/Conferences/2007Meeting/agenda.html, see Bajcy and Watkin presentation.
23. T.E. Cleveland et al., *J. Cereal Sci.* **1** (2008).
24. B. Schillinger et al., private communication.
25. M.A. McDonald and K.L. Watkin, *Acad. Radiol.* **13**(4), 407–536 (2006).
26. M.A. McDonald, K.L. Watkin, *Invest. Radiol.* **38**(6), 305–310 2003.
27. K.L. Watkin, M.A. McDonald, *Acad. Radiol.* **9**(S2), 285–289 (2002).